Revision 1

Olivine from aillikites in the Tarim large igneous province as a window into mantle metasomatism and multi-stage magma evolution

Changhong Wang[1], Zhaochong Zhang[1,*], Qiuhong Xie[1], Zhiguo Cheng[1], Weiliang Kong[1], Bingxiang Liu[1], M. Santosh[1,2], Shengkai Jin[1]

[1]*State Key Laboratory of Geological Processes and Mineral Resources, China University of Geosciences, Beijing 100083, China*

[2]*Department of Earth Sciences, University of Adelaide, SA 5005, Australia*

* Corresponding author

E-mail: zczhang@cugb.edu.cn

Tel: 0086-10-82322195

Fax: 0086-10-82323419

Declarations of interest: none

ABSTRACT

Aillikites are carbonate-rich ultramafic lamprophyres and although they are volumetrically minor components of large igneous province (LIP), these rocks provide important clues to melting and metasomatism in the deep mantle domain during the initial stages of LIPs. In this study, we investigate the Wajilitag 'kimberlites' in the northwestern part of the Tarim LIP which we redefine as hypabyssal aillikites based on the following features: (i) micro-phenocrystic clinopyroxene and Ti-rich andradite garnet occurring in abundance in the carbonate-rich matrix; (ii) Cr-spinel exhibiting typical Fe-Ti enrichment trend also known as titanomagnetite trend; and (iii) olivine showing dominantly low-Mg values (Fo < 90). In order to constrain the magma source and evolution, the major, minor and trace element abundance in olivine grains from these rocks were analyzed using electron microprobe and laser ablation-inductively coupled plasma-mass spectrometry. Olivine in the aillikites occurs as two textural types: (i) groundmass olivines, as sub-rounded grains in matrix; and (ii) macrocrysts, as euhedral-anhedral crystals in nodules. The groundmass olivines show varying Fo_{89-80} with high Ni (1606-3418 ppm) and Mn (1424-2860 ppm) and low Ca (571-896 ppm) contents. In contrast, the macrocrysts exhibit restricted Fo range but a wide range in Ni and Mn. The former occur as phenocrysts, whereas the latter are cognate cumulates that formed from earlier, evolved aillikite melt. The two olivine populations can be further divided into sub-groups, indicating a multi-stage crystallization history of the aillikite melt. The crystallization temperatures of groundmass olivines and macrocrysts in dunite nodules as computed from the spinel-olivine thermometers are 1005-1136°C and

906-1041°C, respectively. The coupled enrichment of Ca and Ti and lack of correlation between Ni and Sc and Co in the olivine grains suggest a carbonate-silicate metasomatized mantle source. Moreover, the high 100*Mn/Fe (average 1.67) at high Ni (up to 3418 ppm), overlapping with OIB olivine, and the 100*Ni/Mg (~1) of primitive Mg-Ni-rich groundmass olivines suggest a mixed source that involved phlogopite- and carbonate-rich metasomatic veins within mantle peridotite.

Keywords: Trace elements; LA-ICP-MS; Olivine; Aillikites; Carbonate-phlogopite metasomatism; Tarim Large Igneous Province

INTRODUCTION

Ultramafic lamprophyres (UMLs) generally mark the earliest magmatic activity in some large igneous provinces (LIPs) (Queen et al. 1996; Riley et al. 2003; Tappe et al. 2006). Aillikites (or carbonate-rich UMLs) are high-Ca (12-20 wt% CaO) and low-Si (22-37 wt% SiO_2) hypabyssal rocks, rich in Mg, Ni, Cr, Ba, Sr, REE and volatiles (Rock 1991; Tappe et al. 2006, 2007, 2008). Although aillikites are volumetrically insignificant in LIPs, their deep-mantle derivation, unique geochemistry and close relationship with diamonds make them potential targets for scientific investigations and economic significance (Tappe et al. 2006; Francis and Patterson 2009; Mitchell and Tappe 2010; Hutchison et al. 2018). The genesis of these ultramafic rocks has remained controversial, primarily because of the uncertainty in the source rock lithology. Petrological and geochemical studies suggest that their formation involved CO_2- and H_2O-rich melting, with the presence of phlogopite and carbonate in the source (Andronikov and Foley 2001; Upton et al. 2006; Foley et al. 2009; Tappe et al. 2017). However, isotope and trace element data seem to indicate a mixed source involving distinct carbonate- and phlogopite-rich veins within depleted peridotite, instead of a homogeneously metasomatized lithospheric mantle (Tappe et al. 2006, 2008; Nasir et al. 2011).

Olivine, the earliest crystalline phase in mantle-derived magmas, acts as a good proxy to evaluate the primitive composition of magmas and their mantle source lithology (Sobolev et al. 2005, 2007; Arndt et al. 2010; De Hoog et al. 2010; Herzberg 2011; Foley et al. 2013; Cordier et al. 2015; Søager et al. 2015; Giuliani and Foley

2016). Forsterite-rich [Fo = 100*Mg/(Fe+Mg) molar] olivine in volcanic rocks, for instance, carries information on the mantle source. The distribution of some elements (Ni, Mn, Co) in olivine, which depends upon the bulk partition coefficient during mantle melting, can be employed to infer the modal abundance of olivine in the residual mantle (Sobolev et al. 2005, 2007; Straub et al. 2008; Foley et al. 2011, 2013). In addition, the content of other trace elements (Ca, Ti, Li, Zn) in olivine, governed dominantly by their primitive content in the source, can be used to decipher the nature of metasomatic agents (Prelević and Foley 2007; Foley et al. 2011, 2013; Prelević et al. 2013; Rooney et al. 2020).

In this paper, we investigate the mineralogy and mineral chemistry of the Wajilitag aillikites in the northwestern part of the Tarim LIP (Fig. 1a). In an earlier study, Wang et al. (1987) classified these ultramafic rocks as 'kimberlites', whereas Bao et al. (2009) proposed that they are not *bona fide* kimberlites due to the lack of typical features of kimberlite such as the absence of mantle xenocrysts and the presence of abundant clinopyroxene and amphibole macrocrysts. In this study, we redefine these rocks as hypabyssal aillikites on the basis of detailed mineralogical and mineral chemical studies. Based on major, minor and trace element compositions of olivine, we evaluate the magma source characteristics and crystallization processes in deep-level magma reservoirs with a view to constrain the petrogenesis of this rare rock type.

GEOLOGICAL SETTING

The Tarim Craton (TC), located in the northwestern part of China (Fig. 1a), consists predominantly of metamorphosed Precambrian crystalline basement and

Phanerozoic sedimentary cover (Long et al. 2010; Zhang et al. 2013a; Xu et al. 2014). The Precambrian basements, mainly exposed in Kuluktage and Aksu, Altyn Tagh and Tieklik and Kunlun (Zhang et al. 2013a), are considered as part of the Columbia and Rodinia supercontinents (Ma et al. 2013a, 2013b; Zhang et al. 2013a). The Phanerozoic strata, which are distributed along the northern margin of the TC, are composed of Ordovician to Neogene sandstones, limestones and volcanosedimentary sequences (Guo et al. 2005; Zhou et al. 2009; Tian et al. 2010). The Cenozoic deformation which extensively modified the tectonic framework of the TC produced three uplifts and four depressions. From north to south, they are the Kuche depression (KD), the Northern Tarim uplift (NTU), the Northern depression (ND), the Central uplift (CU), the Southwestern depression (SD), the Southern Tarim uplift (STU), and the Southeast depression (SD; Jia 1997; Fig. 1a).

Previous studies identified a major Permian thermal event that generated voluminous igneous rocks estimated to be about 300,000 km^2 in the TC, which were assigned as the Tarim large igneous province (TLIP) (Xu et al. 2014; Fig. 1a). The Wajilitag region, located in the northwestern part of the TLIP, is characterized by diverse rock types including carbonate-rich UMLs, carbonatites, mafic-ultramafic intrusions, nephelinites, tephrite dykes, alkaline lamprophyre dykes and syenites (Jiang et al. 2004; Yang et al. 2007; Zhang et al. 2008; Li et al. 2012; Fig. 1b). These rocks intruded the Devonian Keziletag and Yimugangawu strata, which dominantly comprise clastic sequences. Field and geochronological studies have identified the formation sequence of the igneous rocks as follows: carbonate-rich UMLs (300 Ma) → mafic-

ultramafic intrusions (284-281 Ma) → carbonatites and syenites (273 Ma) → tephrite and alkaline lamprophyre dykes → nephelinites (268 Ma) (Zhang et al. 2008; Li et al. 2011; Zhang et al. 2013b; Xu et al. 2014; Cheng et al. 2015).

In the Wajilitag district, 6 pipes and 32 dykes of aillikite have been recognized, which are distributed in the northern portion of this area and generally trend NWW-SEE (Fig. 1b). These carbonate-rich ultramafic bodies attracted considerable interest in the past as the first diamond-bearing rocks in Xinjiang (Du 1983; Guo et al. 2005; Zhang et al. 2008; Cheng et al. 2014). The pipes have elliptical to round shape with dimensions up to 180 m × 100 m (Du 1983; Su 1991). The pipes are cut across by tephrite dykes (Fig. 2a). The dykes are generally 0.5-2 m in width and 5-7 m in length, but the actual length remains uncertain due to desert cover.

PETROGRAPHY

The Wajilitag aillikites exhibit inequigranular porphyritic texture and are distinctively composed of 'nodules' (polygranular aggregates, 10-20%), phenocrysts (30%) and matrix (50-60%) (Fig. 2b-2f). The nodules are dominated by mafic-ultramafic rocks such as dunite (5%), olivine-bearing clinopyroxenite (10%) and clinopyroxenite (85%). These medium- to coarse-grained, holocrystalline textured nodules are composed of olivine and clinopyroxene with subordinate amounts of Cr-spinel (Fig. 2e-2f). The Cr-spinel occurs as euhedral to subhedral grains and is found only in the dunite nodules. The phenocrysts are dominated by olivine (25-30%), clinopyroxene (20-30%), amphibole (15-20%), phlogopite (10-15%), magnetite (5%) and apatite (5%) (Fig. 2c-2d). However, it is difficult to distinguish true phenocrysts as

some of these minerals are probably disaggregation products of the mafic-ultramafic nodules, particularly in the case of olivine and clinopyroxene (Cheng et al. 2014). Furthermore, olivine grains in matrix are usually rounded and abraded in shape, so that it is debated whether they are phenocrysts or xenocrysts (Veter et al. 2017). We classify olivine derived from groundmass and nodules as 'groundmass olivine' and 'macrocrystic olivine', respectively. The matrix has cryptocrystalline texture and consists of calcite (30%), phlogopite (30%), Ti-Fe oxides (5%), perovskite (3%), apatite (4%) and Ti-rich andradite garnet (3%) (Figs. 2g-2i and 3). We observed, for the first time, abundant euhedral clinopyroxene (10-15%), amphibole (10%) and dolomite (5%) micro-phenocryst set in the aillikite matrix (Fig. 3). The presence of primary magmatic clinopyroxene and Ti-rich andradite garnet is considered hallmark mineralogical characteristic of aillikites (Tappe et al. 2005).

ANALYTICAL METHODS

The fresh aillikite samples were collected from 2 pipes and 4 dykes in the northwestern part of the Wajilitag region (Fig. 1b). Quantitative evaluation of minerals using QEMSCAN 650F was used to analyze the minerals in these rocks at the China University of Petroleum, Beijing, following the procedure developed by Benvie (2007) and Hoal et al. (2009). The instrument is an automated quantitative mineralogy tool that utilizes a Carl Zeiss EVO50 SEM platform equipped with four Bruker energy dispersive detectors and a proprietary software to produce false-colored mineral maps from backscatter electron signals and EDS (energy dispersive spectrometer) spectra. The pixel resolution of the images is 1 μm.

Concentrations of major and minor elements of the olivine were obtained with an EMPA1600 electron microprobe at China University of Geosciences, Beijing. Before acquiring the element concentrations, the textures and zoning of olivine samples were analyzed in detail using a Scanning Electron Microscopy (SEM, Zeiss SUPPA 55) equipped with an Oxford energy-dispersive spectrometer (EDS) at China University of Geosciences, Beijing. On the basis of a detailed SEM and EDS investigation of 21 thin sections,112 olivine crystals were selected for EMPA analysis. The operating conditions were 20 kV acceleration voltage, 20 nA beam current, and 5 μm beam diameter, with counting time 10 s (peak) and background counting time 5 s. All elements were measured using Kα1 lines. Natural minerals and synthetic oxides produced by SPI Supplies of the United States are used as standards.

The minor and trace elements were analyzed on a subset of olivines at the National Research Centre for Geoanalysis, Beijing, using an Element 2 Plasma Mass Spectrometer (Thermoscientific, Germany) coupled to a UP 213 laser ablation system (New Wave Research, USA). Details in relation to the LA-ICP-MS technique applied here are described in Hu et al. (2008). ^{29}Si was used as the internal standard for olivine and NIST SRM 610 and USGS GSE-1G as external standards. The laser ablation was run under a helium atmosphere, and argon was applied as the carrier gas. Each analysis was performed by spot diameters varied between 100 and 40 μm at 10 Hz with a fluence of 4.2-6.5 J/cm^2 for 40 s ablation time after measuring the background for 20 s. The preferred values of the element concentrations for the USGS reference glasses are from the GeoReM database (http://georem.mpch-mainz.gwdg.de/, Jochum et al. 2005).

Standard reference materials were run after each 9-10 unknowns. Analytical uncertainty (one sigma) for each spot analysis yielded results consistent within 10%. Instrument precision and standard deviation are listed in Appendix Table S4.

RESULTS

Back-scattered electron (BSE) images and EMPA and LA-ICP-MS analyses show that the majority of groundmass olivines (olivine I) and macrocrysts (olivine II) are homogeneous in composition (Figs. 4a-4c and 5b), whereas macrocrysts in matrix usually comprise homogeneous core and dark high-Mg rind which formed through diffusional re-equilibration (Figs. 4e-4f and 5a). The results of olivine analyses are presented in Appendix Tables S1 and S3.

Major and minor elements

Bivariate element plots help in distinguishing different olivine populations (Shaikh et al. 2019). As shown in Fig. 6a, the Fo vs. Ni diagram illustrates that groundmass olivines define a wide compositional field, extending from Fo_{89-81}, accompanied by a decrease in Ni contents from 3418 to 1606 ppm. The forsterite contents of groundmass olivine extend to values of Fo_{80} (Appendix Table S1). In the Fo vs. Mn diagram (Fig. 6b), most of the data plot on a broad array in which Mn correlates negatively with Fo contents. Additionally, in the plot of Fo vs. Ca (Fig. 6d inset), the Ca concentrations in the high-Mg groundmass olivines (Fo_{85-89}) are 896-598 ppm, and increase gradually from 571 ppm to 781 ppm at decreasing Fo values (Fo_{85-81}). As shown in Fig. 6d, the aspect ratios are low for the high-Mg groundmass olivines (Fo_{85-89}), and increase at decreasing Fo values (Fo_{85-81}), the trend of which is similar to that

of Ca vs. Fo in the groundmass olivine. Based on major and minor element compositions, the groundmass olivines are further divided into high Mg (Fo≥85) and Ni (2300-3418 ppm) and low Mg (Fo<85) and Ni (1606-2300 ppm) subgroups, designated as olivine Ia and Ib.

The macrocrystic olivines, in contrast, show restricted Fo values and variable Ni and Mn concentrations even in a single nodule (Fig. 6a-6c). Macrocrysts (Fo_{83-84}) in dunite nodules (olivine IIa) have higher Ni and Ca contents than macrocrysts (Fo_{76-78}) in olivine-bearing clinopyroxenite nodules (olivine IIb). Mn contents in olivine IIa and IIb are similar. As high-Fo olivine can best reflect the composition of its parental magma, the following discussion focuses on the groundmass olivines (olivine Ia and Ib) and macrocrysts in dunite nodules (olivine IIa).

Trace elements

Quantitative LA-ICP-MS analyses of minor and trace element composition were performed on a subset of macrocrysts and groundmass olivines that were analyzed for major elements. Co-variation of compatible element Ni with other trace elements can be used to constrain the relative behavior of these elements during melt evolution (Howarth 2018). As shown in Fig. 7, Ni is plotted against trace elements including Ca, Ti, Al, Cr, Mn and V for this purpose. Olivine Ia contains relatively higher concentrations of Ca, Al, Cr and V but lower Mn and Ti than olivine Ib (Fig. 7). Olivine IIa has high Ni and low Ti contents overlapping with olivine Ia, whereas the Al, Ca, Cr and V concentrations are significantly lower than olivine Ia. The contents of Mn in olivine IIa are higher than those in olivine Ia. Among the other trace elements, Zn

displays larger variation in olivine Ib (110-218 ppm) compared to olivine Ia (94-147 ppm) and olivine IIa (144-193 ppm) (Fig. 8a). The average Li contents in olivine Ia, Ib and IIa are 3.8 ppm, 4.1 ppm and 5.6 ppm, respectively (Fig. 8a). The concentrations of Sc in olivine Ia, Ib and IIa are 1.9-2.7 ppm, 1.4-3.2 ppm and 1.5-3.2 ppm, respectively (Fig. 8b). Cobalt contents of olivine Ia, Ib and IIa are 135-190 ppm, 155-206 ppm and 166-199 ppm, respectively (Fig. 8c).

DISCUSSION

Classification: aillikites or kimberlites?

Carbonate-rich UMLs are often erroneously classified as kimberlites as a result of similar macroscopic appearance (Rock 1986; Tappe et al. 2005). Compositional differences and the lack of spatial coexistence of contemporaneous aillikites and kimberlites indicate that they are distinct magma types (Rock 1986; Mitchell 1995). Aillikites are characterized by abundant primary groundmass carbonate and in some cases, grade into carbonatites (Tappe et al. 2006). They contain abundant olivine (Fo<90), amphibole and clinopyroxene phenocrysts/micro-phenocrysts, whereas kimberlites are dominated by xenocrystic olivine (Fo>90) and devoid of clinopyroxene phenocrysts (Tappe et al. 2005, 2006). Furthermore, these ultramafic rocks are distinguished from kimberlites by lower MgO, Cr_2O_3 and NiO but higher CaO, Al_2O_3, K_2O, Na_2O, P_2O_5 and CO_2 contents (Rock 1986). Additionally, in contrast to kimberlites, which usually occur within areas of ancient cratons, carbonate-rich UMLs are confined to regions of lithospheric extension (Upton et al. 2006; Nielsen et al. 2009; Tappe et al. 2009, 2018; Rooney et al. 2020). It is notable that both kimberlites and

carbonate-rich UMLs occur in LIPs (e.g. Siberian large igneous province; Nosova et al. 2018).

The Wajilitag carbonate-rich ultramafic rocks were previously referred to as kimberlites (Wang et al. 1987) based on the inequigranular porphyritic texture and occurrence of diamonds. However, Bao et al. (2009) refuted this idea, due to the lack of typical features of kimberlite such as the absence of olivine xenocrysts from mantle and the presence of abundant clinopyroxene and amphibole macrocrysts. In our study, we identify based on detailed mineralogical studies that the rock type has affinities with carbonate-rich UMLs (aillikites). As shown in Figs. 2g and 3, abundant micro-phenocrysts of Ti-rich andradite garnet and clinopyroxene are distributed in the carbonate-rich matrix. Moreover, olivine crystals, occurring in abundance in the aillikites, commonly have compositions of Fo < 90 (Fig. 6). The compositional trend of Cr-spinel (Appendix Table S2) is also consistent with titanomagnetite trend of aillikites in contrast with the magnesian ulvöspinel trend of kimberlites (Mitchell 1986). Finally, they have similar geochemical characteristics with type aillikites from Aillik Bay in Labrador (Appendix Table S5). Therefore, we conclude that the Wajilitag ultramafic rocks are not kimberlites, but aillikites, and we report this rock type for the first time from China.

Temperatures

We estimate the crystallization temperatures of the different olivine populations using the spinel-olivine thermometer calibrated by Coogan et al. (2014). Based on the temperature dependent Al-partitioning between the coexisting high-Mg olivine and Cr-

spinel, the thermometer is independent on the crystallization pressure, oxygen fugacity, melt composition and source lithology (Ballhaus et al. 1991; Wan et al. 2008; Coogan et al. 2014). In addition, the trivalent cation Al diffuses much slower than Mg and Fe in olivine lattice (Spandler and O'Neill 2010). Its content can therefore preserve information on incipient crystallization, even when Fe and Mg have been reset. As olivine and Cr-spinel are the earliest minerals crystallized from the parental melts, the spinel-olivine thermometer provides a precise estimate of the temperature of the most primitive magmas (Coogan et al. 2014). The geothermometer is expressed as follows: $T\ (°\mathrm{C}) = \frac{10^4}{0.575+0.884Cr^{\#}-0.897\ln(K_d)} - 273$, where $Cr^{\#}$ is the ratio of Cr/(Cr + Al) in spinel in atomic proportions, and K_d is ${Al_2O_3}^{olivine}/{Al_2O_3}^{Spinel}$ in wt%. The calculated crystallization temperature for three groundmass olivine grains (olivine Ia and Ib) and five macrocrysts (olivine IIa) are 1005-1136°C and 906-1041°C, respectively.

Origins of the groundmass olivines and macrocrysts: multi-stage crystallization

Olivine in aillikite matrix usually shows rounded and abraded shape, so that it is debated whether they are phenocrysts or xenocrysts from mantle (Veter et al. 2017). Olivine in mantle peridotites is characterized by much lower Ca contents (Thompson and Gibson 2000; Kamenetsky et al. 2008; Sobolev et al. 2008, De Hoog et al. 2010; Bussweiler et al. 2017; Chayka et al. 2020). Along with the presence of melt inclusions and lack of strain texture, we suggest that the sub-rounded groundmass olivines in the Wajilitag aillikites are not accidental mantle xenocrysts. Compared with olivine in mantle peridotites, the groundmass olivines have much lower Ni and higher Mn and Ca

concentrations (average 2193 ppm, 2011 ppm and 696 ppm, respectively). Furthermore, these olivines often contain Cr-spinel inclusions, which have similar compositions with matrix Cr-spinel that crystallized from aillikite melt (Appendix Table S2). Hence, the groundmass olivines may be interpreted as phenocrysts crystallized from aillikite melt (Tappe et al. 2006; Veter et al. 2017; Nosova et al. 2018). In addition, the high Mg-Ni groundmass olivines (olivine Ia) crystallize from more primitive aillikite magma relative to low-Mg-Ni ones (olivine Ib). Olivine Ia interestingly shows rounded shape compared with olivine Ib (Fig. 6d). This observation indicates that olivine Ia formed at a greater depth and experienced significant abrasion and resorption during magma ascent.

Compared with groundmass olivines, the origin of macrocrysts in nodules from carbonate-rich ultramafic rocks is more complex. There are three possibilities for the genesis of these olivine macrocrysts: (1) xenocrysts from Ol-bearing clinopyroxenite intrusions in the Wajilitag area (Li et al. 2001; Bao et al. 2009); (2) mantle-derived xenocrysts (Pilbeam et al. 2013); and (3) cognate crystals termed as 'antecrysts', which describe recycled minerals from a previously solidified crystal mush closely related to the progenitor magmas (Tappe at al. 2006; Veter et al. 2017; Nosova et al. 2018). The first possibility can be ruled out, given that the aillikites predate the formation of the ultramafic intrusions (300 Ma vs. 280 Ma, Zhang et al. 2010; Zhang et al. 2013b). In addition, these olivine macrocrysts (olivine IIa) have lower forsterite (Fo_{83-84}) and Ni (2322-3083 ppm) but higher Mn (1963-2395 ppm) contents in comparison with mantle olivines (Thompson and Gibson 2000; Kamenetsky et al. 2008; Sobolev et al. 2008; De

Hoog et al. 2010; Bussweiler et al. 2017; Chayka et al. 2020). The absence of mantle xenoliths in these aillikites also argues against the possibility that these olivines are xenocrysts derived from the disaggregation of entrained mantle xenoliths. As shown in Fig. 6, olivine IIa shows restricted forsterite values (Fo_{83-84}) but variable Ni and Mn contents. The decoupling of Fo and minor elements (Ni and Mn), usually occurring in olivine rims of kimberlites, is attributable to olivine crystallization from Fe^{2+}-Mg buffered magma, which is possible in the carbonate melt-olivine system (Kamenetsky et al. 2008). In combination with the similar bulk chemical features between the dunite nodules and the host aillikites (Jiang et al. 2004; Sun et al. 2010), we suggest that the third possibility is most likely. The chemistry of olivine IIa is compared with that of the olivine macrocrysts from aillikites of the Aillik Bay and Chadobets areas (Fig. 6). The macrocrysts from these areas are interpreted as crystallization products from earlier, more fractionated batches of aillikite magma (Tappe et al. 2006; Veter et al. 2017; Nosova et al. 2018). Olivine IIa shares similar composition with macrocrysts from the type aillikites of the Aillik Bay and Chadobets areas. We therefore propose that the Fe-rich olivine IIa could be the crystallization product from an earlier, failed batch of aillikite melt that stalled in deep-level magma chambers and experienced significant magma differentiation before being remobilized by new batch of aillikite melt.

Mantle source lithologies of aillikite melts

The composition of aillikites resembles those of experimental melts obtained by melting of mantle peridotite in the presence of both H_2O and CO_2 at 40-60 kbar (Foley et al. 2009), although these cannot be melts of peridotite alone (Tappe et al. 2006).

Mineralogy of mantle sources can be deduced from minor and trace element in olivine over a range of igneous rocks, including basalts (Hagerty et al. 2006; Sobolev et al. 2007), lamproites (Ammannati et al. 2016; Shaikh et al. 2019; Chayka et al. 2020), kimberlites (Bussweiler et al. 2015; Howarth 2018; Jaques and Foley 2018; Nosova et al. 2018) and aillikites (Veter et al. 2017; Nosova et al. 2018; Rooney et al. 2020). In this section, we will use minor elements (Ni, Mn, Ca), combined with trace elements (Li, Zn, Sc, Ti, Co), in olivine to discriminate between pyroxenitic and peridotitic mantle source lithologies and identify different metasomatic agents in the source.

Modal content of olivine in mantle source. As shown in Fig. 6a, olivine Ia, Ib and IIa are Ni-enriched (average 2756, 1960 and 2649 ppm, respectively) and overlap with the field for olivine from pyroxenite-derived ocean island basalts (OIB). However, the high Mn concentrations of olivine Ia, Ib and IIa (average 1651, 2160 and 2202 ppm, respectively) are more similar to peridotite-derived mid ocean ridge basalts (MORB) than OIB (Fig. 6b). In the Fo vs. Ca plot (Fig. 6c), the Ca contents of olivine Ia, Ib and IIa (average 754, 673 and 653 ppm, respectively) are markedly lower than olivine from MORB and OIB. Recent research showed that Ca olivine-melt partitioning is significant affected by the content of H_2O and CO_2 in the melt, whereby at higher H_2O and CO_2 contents, olivine-melt partition coefficient for Ca is significantly lowered (Feig et al. 2006; Gavrilenko et al. 2016). For example, olivine Ca contents in some subduction-related magmas (Fig. 6c) are low (< 1000 ppm) relative to typical MORB and OIB magmas (> 1100 ppm) (Kamenetsky et al. 2006; Søager et al. 2015; Gavrilenko et al. 2016; Zamboni et al. 2017). Thus, the low-Ca contents of olivine Ia,

Ib and IIa probably resulted from the high H_2O and CO_2 contents of aillikite magmas.

High Mn concentrations in olivine have been explained by two mechanisms: (1) low MgO contents in parent magmas (Matzen et al. 2017); and (2) parent magmas derived from peridotite source (Sobolev et al. 2007). Considering the high MgO contents of the Wajilitag aillikites (up to 21 wt%), we propose that the Mn-rich feature of olivine Ia, Ib and IIa is probably related to the second mechanism. In addition, since olivine is the only mantle silicate phase with $D^{ol\text{-}liq}Fe > D^{ol\text{-}liq}Mn$ (1.09 vs. 0.89), partial melting of peridotite source will release more Mn than olivine-poor one. Thus, olivine crystallized from melts derived from a peridotite source generally have high 100*Mn/Fe (1.6-2.0; Sobolev et al. 2007; Foley et al. 2013). As shown in Fig. 9, the 100*Mn/Fe of olivine Ia (average 1.67) crystallized from primitive aillikite magma is similar to that for olivine in equilibrium with peridotite derived melts. Additionally, olivine derived from peridotite source also tends to have high Mn/Zn ratios (>14; Howarth and Harris 2017). The average Mn/Zn ratio of olivine Ia is 14.2. Therefore, the olivine chemistry of the Wajilitag aillikites is generally more consistent with a peridotite-dominated source, despite the high Ni contents.

Constraints on mantle metasomatic agents. High Ni contents of olivine might be because of three main processes: (1) olivine crystallized at low P-T conditions (Matzen et al. 2017); (2) magma sourced from 'dry' pyroxenite or phlogopite pyroxenite source (Sobolev et al. 2007; Ammannati et al. 2016); and (3) olivine chemistry inherited from metasomatic materials in the source (Veter et al. 2017; Howarth 2018; Rooney et al. 2020). The high Ni contents of olivine Ia, Ib and IIa cannot

result from the first factor, considering their high P crystallizing condition (4.5 GPa, Su 1991).

As illustrated in Fig 8a-8c, the chemical data of olivine Ia, Ib and IIa are plotted in comparison aillikites of the Aillik Bay area and fields for phlogopite pyroxenite and 'dry' pyroxenite (Sobolev et al. 2007; Ammannati et al. 2016). In addition, a field for olivine in continental alkaline volcanics is outlined on the basis of the chemistry of olivine in ugandites, kimberlites, melilitites and basanites (Foley et al. 2013; Veter et al. 2017; Nosova et al. 2018). Such alkaline magmas have been interpreted to originate from melting of metasomatized mantle sources (Foley et al. 2013; Howarth 2018). The chemistry of olivine Ia, Ib and IIa shows no evidence for 'dry' pyroxenite or phlogopite pyroxenite source. Instead, they are closely grouped together with olivine from aillikites and continental alkaline rocks, consistent with a significant contribution from metasomatic components in source.

The Ca vs. Ti (log) element variation, as shown in Fig. 8d, can be used to discriminate between different metasomatic agents in the mantle source (Foley et al. 2013; Veter et al. 2017). For instance, owing to carbonate-silicate melt metasomatism in mantle, olivines from rift-related volcanics of East Africa show coupled elevation of Ca and Ti (black arrow). In contrast, craton peridotites have olivines with high Ti but little or no increase in Ca (South Africa and Canada, grey arrow), which is ascribed to Ti-Fe-rich silicate melt metasomatism. The chemistry of olivine Ia, Ib and IIa shows a greater tendency to higher Ca contents resembling type aillikites and rift-related volcanics (Fig. 8d), indicating the presence of carbonate-silicate metasomatic materials

in the source. Moreover, the carbonate-rich nature of the Wajilitag aillikites and a recent study that reported Sr-Nd-C-O and Mg isotope data (Cheng et al. 2018) are also consistent with this inference.

Several previous studies have suggested that the chemistry of olivine in aillikites is controlled by phlogopite (± carbonate) in the mantle source (Tappe et al. 2006; Veter et al. 2017; Nosova et al. 2018). The high Ni contents, overlapping OIB basalt olivine sourced from pyroxenite-derived melts, and 100*Ni/Mg of ~1 for olivine phenocrysts in aillikites are thought to inherit from phlogopite in the source. In Fig. 9, the chemistry of olivine Ia crystallized from primitive melt of the Wajilitag aillikite is compared with that of olivine phenocrysts reported by Veter et al. (2017) and Nosova et al. (2018). In addition, we also compare the olivine Ia chemistry reported in this study with the olivine chemistry of orangeites (also known as Group II kimberlites) from southern Africa, which are known to have been derived from melting of a phlogopite metasomatized mantle sources (Becker and Le Roex 2006). Olivine Ia has 100*Ni/Mg values (~1) similar to olivine in type aillikites and early crystallized olivine in orangeites, whereas its high 100*Mn/Fe ratios (1.5-1.8) are more similar to olivine from peridotite-derived magmas. Therefore, the chemical composition of primitive olivine Ia is indicative of a mixed source involving phlogopite-rich veins within a depleted mantle peridotite.

In summary, the chemistry of Ia, Ib and IIa, coupled with the carbonate-rich nature of the Wajilitag aillikites and previous bulk-rock isotope data (Cheng et al. 2018), suggests that these ultramafic rocks were derived from a peridotite source metasomatized by carbonate and phlogopite. The elevated Ni contents, overlapping

with OIB olivine, and 100*Ni/Mg of ~1 may be inherited from phlogopite in the source, whereas the high 100*Mn/Fe and Mn/Zn indicate that the source is dominated by peridotite.

Implications for the petrogenesis of the Wajilitag aillikites

Based on the discussion above, it can be concluded that carbonate- and phlogopite-rich metasomatic components may have played an important role in the formation of the primary melt of Wajilitag aillikite. Moreover, the presence of four generations of olivine in the aillikites suggests that these magmas have experienced multi-stage crystallization processes in deep-level magma reservoirs. Olivine IIa and IIb crystallized from earlier, evolved aillikitic melt, whereas olivine Ia and Ib sourced from late stage aillikitic melt. The Mg-Ni-rich olivine Ia originated from greater depth and was related to more primitive aillikite magma relative to Mg-Ni-poor olivine Ib.

A three-stage model, as shown in Fig. 10, is proposed to interpret the petrogenesis of the Wajilitag aillikites which involves the following processes. (1) Asthenospheric H_2O- and CO_2-rich components froze at the base of the cratonic lithosphere to form carbonate-phlogopite metasomatic veins (Tappe et al. 2006, 2007). Re-melting of these veins, during the initial impingement of the TLIP at ~300 Ma (Zhang et al. 2013b), contributed to the volatile-fluxed melting of ambient peridotite and produced proto-aillikite melts; (2) The early batches of melts, however, failed to erupt and were stagnated in deep-level magma chambers. The presence of abundant nodules (Figs. 2e-2f and 4d-4e) in the samples indicates that these magma reservoirs are partly crystallized crystal-melt mushes. (3) Subsequently, large volumes of ascending aillikite

magmas crystallized olivine Ia and Ib, as well as entrained and remobilized the early formed olivine IIa and IIb.

IMPLICATIONS

The Wajilitag 'kimberlites' in the northwestern part of the Tarim LIP were redefined as hypabyssal aillikites in this study based on the following features: (1) micro-phenocrystic clinopyroxene and Ti-rich andradite garnet occurring in abundance in the carbonate-rich matrix; (2) Cr-spinel exhibiting typical Fe-Ti enrichment trend also known as titanomagnetite trend; and (3) olivine showing dominantly low-Mg values (Fo < 90). Hence, this is the first time for the rock type to be reported from China.

Olivines are common in the aillikites. Based on detailed textural and mineralogical studies, these olivines are divided in two groups: 1) macrocrysts, as euhedral-anhedral crystals in nodules; and 2) groundmass olivines, as sub-rounded grains in matrix. Moreover, the two olivine populations can be further divided into sub-groups, indicating a multi-stage crystallization history of the aillikite melt. The macrocrysts were produced in deep-level magma chamber by one or more batch of aillikite melt before being recycled and transported to Earth's surface by new batch of aillikite magma. Similar olivine macrocrysts were also reported in the aillikites of the Aillik Bay and Chadobets areas, suggesting that failed aillikite intrusions are probably a common phenomenon. The groundmass olivines are phenocrysts crystallized from the host aillikite magma. The Mg-Ni-rich groundmass olivines originated from greater depth and were related to more primitive aillikite magma relative to Mg-Ni-poor ones.

Finally, by applying the geochemistry of olivine in identifying mantle source

lithologies, we suggest that the commonly-accepted mechanism of origin of an aillikite is also applicable to the Wajilitag aillikites. However, the factors that control olivine chemistry in such magmas are still poorly-understood, and thus further studies are required in future.

ACKNOWLEDGEMENT

The authors would like to acknowledge Yanru Zhang, Dongjie Tang, Jinwu Yin and Linghao Zhao for their technical support. We are grateful to Don Baker, Charles Lesher, Sebastian Tappe and an anonymous referee for their helpful suggestions and constructive comments on this manuscript. Geoffrey Howarth, Anna Nosova, Xianghui Fei and Mpoho Martial are appreciated for their constructive suggestions. Financial support for this work was supported by the National Natural Science Foundation of China (No.41472060 and No. 41702064).

REFERENCES CITED

Ammannati, E., Jacob, D.E., Avanzinelli, R., Foley, S.F., and Conticelli, S. (2016) Low Ni olivine in silica-undersaturated ultrapotassic igneous rocks as evidence for carbonate metasomatism in the mantle. Earth and Planetary Science Letterss, 444, 64-74.

Andronikov, A.V., and Foley, S.F. (2001) Trace element and Nd-Sr isotopic composition of ultramafic lamprophyres from the East Antarctic Beaver Lake area, Chemical Geologu, 175, 291-305.

Arndt, N.T., Guitreau, M., Boullier, A.M., Le Roex, A., Tommasi, A., Cordier, P., and Sobolev, A. (2010) Olivine and the origin of kimberlite. Journal of Petrology, 51, 573-602.

Ballhaus, C.B., Berry, R.F., and Green, D.H. (1991) High pressure experimental calibration of the olivine-orthopyroxene-spinel oxygen barometer-implications for

redox conditions in the Upper mantle. Contributions to Mineralogy and Petrology, 107, 27-40

Bao, P.S., Su, L., Zhai, Q.G., and Xiao, X.C. (2009) Compositions of the kimberlitic brecciated peridotite in the Bachu area, Xinjiang and its ore-bearing potentialities. Acta Geologica Sinica, 83, 1276-1301 (in Chinese with English abstract).

Becker, M., and Le Roex, A.P. (2006) Geochemistry of south African on-and off-craton, group I and group II kimberlites: petrogenesis and source region evolution. Journal of Petrology, 47(4), 673-703.

Benvie, B. (2007) Mineralogical imaging of kimberlites using SEM-based techniques. Minerals Engineering, 20(5), 435-443.

Bussweiler. Y., Foley, S.F., Prelević, D., and Jacob, D.E. (2015) The olivine macrocryst problem: new insights from minor and trace element compositions of olivine from Lac de Gras kimberlites, Canada. Lithos, 220-223, 238-252.

Bussweiler, Y., Brey, G.P., Pearson, D.G., Stachel, T., Stern, R.A., Hardman, M.F., Kjarsgaard, B.A., and Jackson, S.E. (2017) The aluminum-in-olivine thermometer for mantle peridotites—Experimental versus empirical calibration and potential applications. Lithos, 272, 301-314.

Chayka, I.F., Sobolev, A.V., Izokh, A.E., Batanova, V.G., Krasheninnikov, S.P., Chervyakovskaya, M.V., Kontonikas-Charos, A., Kutyrev, A.V., Lobastov, B.M., and Chervyakovskiy, V.S. (2020) Fingerprints of Kamafugite-Like Magmas in Mesozoic Lamproites of the Aldan Shield: Evidence from Olivine and Olivine-Hosted Inclusions. Minerals, 10(4), 337.

Cheng, Z.G., Zhang, Z.C., Santosh, M., Hou, T., Zhang, D.Y. (2014) Carbonate- and silicate-rich globules in the kimberlitic rocks of northwestern Tarim large igneous province, NW China: Evidence for carbonated mantle source. Journal of Asian Earth Sciences, 95, 114-135.

Cheng, Z.G., Zhang, Z.C., Hou, T., Santosh, M., Zhang, D.Y., and Ke, S. (2015) Petrogenesis of nephelinites from the Tarim Large Igneous Province, NW China: Implications for mantle source characteristics and plume-lithosphere interaction. Lithos, 220-223, 164-178.

Cheng, Z.G., Zhang, Z.C., Xie, Q.H., Hou, T., and Ke, S. (2018) Subducted slab-plume interaction traced by magnesium isotopes in the northern margin of the Tarim Large Igneous Province. Earth and Planetary Science Letters, 489, 100-110.

Coogan, L.A., Saunders, A.D., and Wilson, R.N. (2014) Aluminum-in-olivine thermometry of primitive basalts: evidence of an anomalously hot mantle source for large igneous provinces. Chemical Geology, 368, 1-10.

Cordier, C., Sauzeat, L., Arndt, N.T., Boullier, A-M., Batanova, V., and Barou, F. (2015) Metasomatism of the lithospheric mantle immediately precedes kimberlite eruption: new evidence from olivine composition and microstructures. Journal of Petrology, 56, 1775-1796.

De Hoog, J.C.M., Gall, L., and Cornell, D.H. (2010) Trace-element geochemistry of mantle olivine and application to mantle petrogenesis and geothermobarometry. Chemical Geology, 270, 196-215.

Du, P.L. (1983) Brief introduction of geological characters of kimberlite body at

Wajilitag in Bachu County, Xinjiang. Xinjiang Geology, 1, 55-64. (in Chinese with English abstract).

Feig, S.T., Koepke, J., and Snow, J.E. (2006) Effect of water on tholeiitic basalt phase equilibria: an experimental study under oxidizing conditions. Contributions to Mineralogy and Petrology, 152(5), 611-638.

Foley, S.F., Yaxley, G.M., Rosenthal, A., Buhre, S., Kiseeva, E.S., Rapp, R.P., and Jacob, D.E. (2009) The composition of near-solidus melts of peridotite in the presence of CO_2 and H_2O between 40 and 60 kbar. Lithos, 112S, 274-283.

Foley, S.F., Jacob, D.E., and O'Neill, H.S.C. (2011) Trace element variations in olivine phenocrysts from Ugandan potassic rocks as clues to the chemical characteristics of parental magmas. Contributions to Mineralogy and Petrology, 162, 1-20.

Foley, S.F., Prelević, D., Rehfeldt, T., and Jacob, D.E. (2013) Minor and trace elements in olivines as probes into early igneous and mantle melting processes. Earth and Planetary Science Letters, 363, 181-191.

Francis, D., and Patterson, M. (2009) Kimberlites and aillikites as probes of the continental lithospheric mantle. Lithos, 109, 72-80.

Fritschle, T., Prelević, D., Foley, S.F., and Jacob, D.E. (2013) Petrological characterization of the mantle source of Mediterranean lamproites: indications from major and trace elements of phlogopite. Chemical Geology, 353, 267-279.

Gavrilenko, M., Herzberg, C., Vidito, C., Carr, M.J., Tenner, T., and Ozerov, A. (2016) A calcium in-olivine geohygrometer and its application to subduction zone magmatism. Journal of Petrology, 57(9), 1811-1832.

Giuliani, A., and Foley, S.F. (2016) The geochemical complexity of kimberlite rocks and their olivine populations: a comment on Cordier et al. (Journal of Petrology, 56, 1775–1796, 2015). Journal of Petrology, 57, 927-932.

Guo, Z.J., Yin, A., Robinson, A., and Jia, C.Z. (2005) Geochronology and geochemistry of deep drill-core samples from the basement of the central Tarim basin. Journal of Asian Earth Sciences, 25, 45-56.

Hagerty, J.J., Shearer, C.K., Vaniman, D.T., and Burger, P.V. (2006) Identifying the effects of petrologic processes in a closed basaltic system using trace-element concentrations in olivines and glasses: implications for comparative planetology. American Mineralogist, 91, 1499-1508.

Herzberg, C. (2011) Identification of source lithology in the Hawaiian and Canary Islands: implications for origins. Journal of Petrology, 52, 113-146.

Hoal, K.O., Appleby, S.K., Stammer, J.G., and Palmer, C. (2009) SEM-based quantitative mineralogical analysis of peridotite, kimberlite, and concentrate. Lithos, 112, 41-46.

Howarth, G.H. (2018) Olivine megacryst chemistry, Monastery kimberlite: Constraints on the mineralogy of the HIMU mantle reservoir in southern Africa. Lithos, 314-315, 658-668.

Howarth, G.H., and Harris, C. (2017) Discriminating between pyroxenite and peridotite sources for continental flood basalts (CFB) in southern Africa using olivine chemistry. Earth and Planetary Science Letters, 475, 143-151.

Hu, M.Y., He, H.L., Zhan, X.C., Fan, X.T., Wang, G., and Jia, Z.R. (2008) Matrix

normalization for in situ multi element quantitative analysis of zircon in laser ablation inductively coupled plasma mass spectrometry. Chinese Journal of Analytical Chemistry, 36, 947-953.

Hutchison, M.T., Faithfull, J.W., Barfod, D.N., Hughes, J.W., and Upton, B.G.J. (2018) The mantle of Scotland viewed through the Glen Gollaidh aillikite. Mineralogy and Petrology, 112S, S115-S132.

Jia, C.Z. (1997) Tectonic Characteristics and Oil-Gas in the Tarim Basin, China. Petroleum Industry Press, Beijing (in Chinese).

Jiang, C.Y., Zhang, P.B., Lu, D.R., and Bai, K.Y. (2004) Petrogenesis and magma source of the ultramafic rocks at Wajilitag region, western Tarim Plate in Xinjiang. Acta Petrologica Sinica, 20, 1433-1444 (in Chinese with English abstract).

Jaques, A.L., and Foley, S.F. (2018) Insights into the petrogenesis of the West Kimberley lamproites from trace elements in olivine. Mineralogy and Petrology, 112(2):519-537.

Jochum. K.P., Nohl, U., Herwig, K., Lammel, E., Stoll, B., and Hofmann, A.W. (2005) GeoReM: a new geochemical database for reference materials and isotopic standards. Geostandards and Geoanalytical Research, 29, 333-338.

Kamenetsky, V.S., Elburg, M., Arculus, R., and Thomas, R. (2006) Magmatic origin of low-ca olivine in subduction-related magmas: co-existence of contrasting magmas. Chemical Geology, 233(3), 346-357.

Kamenetsky, V.S., Kamenetsky, M.B., Sobolev, A.V., Alexander V.G., Sylvie, D., Kevin, F., Victor V.S., and Dmitry V.K. (2008) Olivine in the Udachnaya-East kimberlite

(Yakutia, Russia): types, compositions and origins. Journal of Petrology, 49, 823-839.

Li, C.N., Lu, F.X., and Chen, M.H. (2001) Research on petrology of the Wajilitag complex body in north edge in the Talimu basin. Xinjiang Geology, 19, 38-42. (in Chinese with English abstract).

Li, Z.L., Chen, H.L., Song, B., Li, Y.Q., Yang, S.F., and Yu, X. (2011) Temporal evolution of the Permian large igneous province in Tarim Basin, Northwest China. Journal of Asian Earth Sciences, 42, 917-927.

Li, Z.L., Li, Y.Q., Chen, H.L., Santosh, M., Yang, S.F., Xu, Y.G., Langmuir, C.H., Chen, Z.X., Yu, X., and Zou, S.Y. (2012) Hf isotopic characteristics of the Tarim Permian large igneous province rocks of NW China: implication for the magmatic source and evolution. Journal of Asian Earth Sciences, 49, 191-202.

Long, X.P., Yuan, C., Sun, M., Zhao, G.C., Xiao, W.J., Wang, Y.J., Yang, Y.H., and Hu, A.Q. (2010) Archean crustal evolution of the northern Tarim Craton, NW China: zircon U-Pb and Hf isotopic constraints. Precambrian Research, 180, 272-284.

Ma, X.X., Shu, L.S., Santosh, M., and Li, J.Y. (2013a) Paleoproterozoic collisional orogeny in Central Tianshan: assembling the Tarim Block within the Columbia supercontinent. Precambrian Research, 228, 1-19.

Ma, X.X., Shu, L.S., and Meert, J.G. (2013b) Early Permian slab breakoff in the Chinese Tianshan belt inferred from the post-collisional granitoids. Gondwana Research, 27, 228-243.

Matzen, A.K., Wood, B.J, Baker, M.B., and Stolper, E.M. (2017) The roles of

pyroxenite and peridotite in the mantle sources of oceanic basalts. Nature geoscience, 12, 530-539.

Mitchell, R.H. (1986) Kimberlites: Mineralogy, Geochemistry and Petrology. Plenum, New York.

Mitchell, R.H. (1995) Kimberlites, orangeites, and related rocks. Plenum, New York.

Mitchell. R., and Tappe, S. (2010) Discussion of "kimberlites and aillikites as probes of the continental lithospheric mantle", by D. Francis and M. Patterson (Lithos v. 109, p. 72-80). Lithos, 115, 288-292.

Nasir, S., Al-Khirbash, S., Rollinson, H., Al-Harthy, A., Al-Sayigh, A., Al-Lazki, T.T., Massonne, H.J., and Belousova, E. (2011) Petrogenesis of early cretaceous carbonatite and ultramafic lamprophyres in a diatreme in the Batain Nappes, Eastern Oman continental margin. Contributions to Mineralogy and Petrology, 161, 47-74.

Nielsen, T.F.D., Jensen, S.M., Secher, K., and Sand, K.K. (2009) Distribution of kimberlite and aillikite in the Diamond Province of southernWest Greenland: a regional perspective based on groundmass mineral chemistry and bulk compositions. Lithos, 112S, 358-371.

Nosova, A.A., Sazonova, L.V., Kargin, A.V., Smirnova, M.D., Lapin, A.V., and Shcherbakov, V.D. (2018) Olivine in ultramafic lamprophyres: chemistry, crystallisation, and melt sources of Siberian Pre- and post-trap aillikites. Contributions to Mineralogy and Petrology, 173, 55.

Pilbeam, L.H., Nielsen, T.F.D., and Waight, T.E. (2013) Digestion fractional

crystallization (DFC): an important process in the genesis of Kimberlites. Evidence from Olivine in the Majuagaa Kimberlite, Southern West Greenland. Journal of Petrology, 54, 1399-1425.

Prelević, D., and Foley, S.F. (2007) Accretion of arc-oceanic lithospheric mantle in the Mediterranean: evidnence from extremely high-Mg olivines and Cr-rich spinel inclusions from lamproites. Earth and Planetary Science Letters, 256, 120-135.

Prelević, D., Jacob, D.E., and Foley, S.F. (2013) Recycling plus: a new recipe for the formation of Alpine—Himalayan orogenic mantle lithosphere. Earth and Planetary Science Letters, 362, 187-197.

Queen, M., Heaman, L.M., Hanes, J.A., Archibald, D.A., and Farrar, E. (1996). 40Ar/39Ar phlogopite and U-Pb perovskite dating of lamprophyre dykes from the eastern Lake Superior region: evidence for a 1.14 Ga magmatic precursor to Midcontinent Rift volcanism. Canadian Journal of Earth Sciences, 33, 958-965.

Riley, T.R., Leat, P.T., Storey, B.C., Parkinson, I.J., and Millar, I.L. (2003). Ultramafic lamprophyres of the Ferrar large igneous province: evidence for a HIMU mantle component. Lithos, 66, 63-76.

Rock, N.M.S. (1986) The nature and origin of ultramafic lamprophyres: alnöites and allied rocks. Journal of Petrology, 27, 155-196.

Rock, N.M.S. (1991) Lamprophyres. Glasgow, Blackie.

Rooney, T.O., Girard, G., and Tappe, S. (2020) The impact on mantle olivine resulting from carbonated silicate melt interaction. Contributions to Mineralogy and Petrology, 175, 56-71.

Shaikh, A.M., Patel, S.C., Bussweiler, Y., Kumar, S.P., Tappe, S., Ravi, S., and Mainkar, D. (2019) Olivine trace element compositions in diamondiferous lamproites from India: Proxies for magma origins and the nature of the lithospheric mantle beneath the Bastar and Dharwar cratons. Lithos, 324-325, 501-518.

Søager, N., Portnyagin, M., Hoernle, K., Holm, P.M., Hauff, F., and Garbeschönberg, D. (2015) Olivine major and trace element compositions in southern Payenia basalts, Argentina: evidence for pyroxenite-peridotite melt mixing in a back-arc setting. Journal of Petrology, 56, 1495-1518.

Sobolev, A.V., Hofmann, A.W., Sobolev, S.V., and Nikogoslan, I.K. (2005) An olivine-free mantle source of Hawaiian sheild basalts. Nature, 434, 590-597.

Sobolev, A.V., Hofmann, A.W., Kuzmin, D.V. Yaxley, G.M., Arndt, N.T., Chung, S.L., Danyushevsky, L.V., Elliott, T., Frey, F.A., Garcia, M.O., and others (2007) The amount of recycled crust in sources of mantle-derived melts. Science, 316, 412-417.

Sobolev, N.V., Logvinova, A.M., Zedgenizov, D.A., Pokhilenko, N.P., Kuzmin, D.V., and Sobolev, A.V. (2008) Olivine inclusions in Siberian diamonds: high-precision approach to minor elements. European Journal of Mineralogy, 20, 305-315.

Spandler, C., and O'Neill, H.S.C. (2010) Diffusion and partition coefficients of minor and trace elements in San Carlos olivine at 1300°C with some geochemical implications. Contributions to Mineralogy and Petrology, 159, 791-818.

Straub, S.M., LaGatta, A.B., Martin-Del Pozzo, A.L., and Langmuir, C.H. (2008) Evidence from high-Ni olivines for a hybridized peridotite/pyroxenite source for orogenic andesites from the central Mexican Volcanic Belt. Geochemistry

Geophysics Geosystems 9(3), Q03007.

Su, L. (1991) A research on magmatic inclusions in minerals from kimberlite in Bachu County, Xinjiang, China. Northwest Geoscience, 32, 15-33 (in Chinese with English abstract).

Sun, L.H. (2010) Geochemical Inversion of the Wajilitag Ultramafic Rocks in Tarim Basin, NW China. Journal of Jilin University (Earth Science Edition), 40, 1302-1322

Tappe, S., Foley, S.F., Jenner, G.A., and Kjarsgaard, B.C. (2005) Integrating ultramafic lamprophyres into the IUGS classification of igneous rocks: rationale and implications. Journal of Petrology, 46, 1893-2000.

Tappe, S., Foley, S.F., Jenner, G.A., Heaman, L.M., Kjarsgaard, B.A., Romer, R.L., Stracke, A., Joyce, N., and Hoefs, J. (2006) Genesis of ultramafic lamprophyres and carbonatites at Aillik Bay, labrador: a consequence of incipient lithospheric thinning beneath the North Atlantic Craton. Journal of Petrology, 47, 1261-1315.

Tappe, S., Foley, S.F., Stracke, A., Romer, R.L., Heaman, L.M., Kjarsgaard, B.A., and Joyce, N. (2007). Craton reactivation on the Labrador Sea margins: $^{40}Ar/^{39}Ar$ age and Sr-Nd-Hf-Pb isotope constraints from alkaline and carbonatite intrusives. Earth and Planetary Science Letters, 256, 433-454.

Tappe, S., Foley, S.F., Kjarsgaard, B.A., Kjarsgaard, B.A., Romer, R.L., Heaman, L.M., Stracke, A., and Jenner, G.A. (2008) Between carbonatite and lamproite—Diamondiferous Torngat ultramafic lamprophyres formed by carbonate-fluxed melting of cratonic MARID-type metasomes. Geochimica Et Cosmochimica Acta,

72, 3258-3286.

Tappe, S., Steenfelt, A., Heaman, L.M., and Simonetti, A. (2009) The newly discovered Jurassic Tikiussaq carbonate-aillikite occurrence, West Greenland, and some remarks on carbonatite-kimberlite relationships. Lithos, 112S, 385-399.

Tappe, S., Romer, R.L., Stracke, A., Steenfelt, A., Smart, K.A., Muehlenbachs, K., and Torsvik, T. H. (2017). Sources and mobility of carbonate melts beneath cratons, with implications for deep carbon cycling, metasomatism and rift initiation. Earth and Planetary Science Letters, 466, 152-167.

Tappe, S., Smart, K., Torsvik, T., Massuyeau, M., and de Wit, M. (2018) Geodynamics of kimberlites on a cooling Earth: clues to plate tectonic evolution and deep volatile cycles. Earth and Planetary Science Letters, 484, 1-14.

Thompson, R.N., and Gibson, S.A. (2000) Transient high temperatures in mantle plume heads inferred from magnesian olivines in Phanerozoic picrites. Nature, 407, 502-506.

Tian, W., Campbell, I.H., Allen, C.M., Guan, P., Pan, W.Q., Chen, M.M., Yu, H.J., and Zhu, W.P. (2010) The Tarim picrate-basalt-rhyolite suite, a Permian flood basalt from northwest China with contrasting rhyolites produced by fractional crystallization and anatexis. Contributions to Mineralogy and Petrology, 160, 407-425.

Upton, B.G.J., Craven, J.A., and Kirstein, L.A. (2006) Crystallization of mela-aillikites of the Narsaq region, Gardar alkaline province, south Greenland and relationships to other aillikitic-carbonatitic associations in the province. Lithos, 92, 300-319.

Veter, M., Foley, S.F., Mertz-Kraus, R., and Groschopf, N. (2017) Trace elements in olivine of ultramafic lamprophyres controlled by phlogopite- rich mineral assemblages in the mantle source. Lithos, 292-293, 81-95.

Wan, Z., Coogan, L.A., and Canil, D. (2008) Experimental calibration of aluminum partitioning between olivine and spinel as a geothermometer. American Mineralogist, 93, 1142-1147.

Wang, Y.S., and Su, L. (1987) A discussion on petrological and mineralogical characteristics of kimberlitic rock in Bachu County, Xinjiang, China and a comparison with some other kimberlitic occurrences. Northwest Geoscience, 15, 47-56 (in Chinese with English abstract).

Xu, Y.G., Wei, X., Luo, Z.Y., Liu, H.Q., and Gao, J. (2014) The Early Permian Tarim large igneous province: Main characteristics and a plume incubation model. Lithos, 204, 20-35.

Yang, S.F., Li, Z., Chen, H., Santosh, M., Dong, C.W., and Yu, X. (2007) Permian bimodal dyke of Tarim Basin, NW China: geochemical characteristics and tectonic implications. Gondwana Research, 12, 113-120.

Zamboni, D., Trela, J., Gazel, E., Sobolev, A.V., Cannatelli, C., Lucchi, F., and De Vivo, B. (2017) New insights into the Aeolian Islands and other arc source compositions from highprecision olivine chemistry. Lithos, 272, 185-191.

Zhang, C.L., Li, X.H., Li, Z.X., Ye, H.M., and Li, C.N. (2008) A Permian layered intrusive complex in the Western Tarim Block, Northwestern China: product of a Ca. 275Ma mantle plume? The Journal of Geology, 116, 269-287.

Zhang, C.L., Xu, Y.G., Li, Z.X., Wang, H.Y., and Ye, H.M. (2010) Diverse Permian magmatism in the Tarim Block, NW China: genetically linked to the Permian Tarim mantle plume? Lithos, 119, 537-552.

Zhang, C.L., Zou, H.B., Li, H.K., and Wang, H.Y. (2013a) Tectonic framework and evolution of the Tarim Block in NW China. Gondwana Research, 23, 1306-1315.

Zhang, D.Y., Zhang, Z.C., Santosh, M., Cheng, Z.G., Huang, H., and Kang, J.L. (2013b) Perovskite and baddeleyite from kimberlitic intrusions in the Tarim large igneous province signal the onset of an end-Carboniferous mantle plume. Earth and Planetary Science Letters, 361(1), 238-248.

Zhou, M.F., Zhao, J.H., Jiang, C.Y., Gao, J.F., Wang, W., and Yang, S.H. (2009) OIB-like, heterogeneous mantle sources of Permian basaltic magmatism in the western Tarim Basin, NW China: implications for a possible Permian large igneous province. Lithos, 113, 583-594.

Figure Captions

FIGURE 1. (**a)** Schematic map of the Tarim Large Igneous Province showing the distribution of the magmatic units including flood basalts, rhyolites and related intrusions (after Xu et al. 2014). (**b)** Detailed geological map of the Wajilitag area that shows the location of carbonate-rich UMLs (after Cheng et al. 2015).

FIGURE 2. (**a)** Field photograph of the Wajilitag aillikite intruded by tephrite dyke. (**b)** Olivine macrocrysts in the aillikite hand specimen. (**c)** Inequigranular porphyritic textured aillikites comprising abundant olivine, phlogopite, amphibole and clinopyroxene, plane-polarized light. (**d)** Same as c, but in cross-polarized light. (**e)** Dunite nodule mainly consisting of olivine and minor Cr-spinel, plane-polarized light. (**f)** Olivine-bearing clinopyroxenite nodule. Euhedral olivine macrocrysts disseminate in interstitial space between clinopyroxene, plane-polarized light. (**g-h)** Amphibole and phlogopite distributed in the carbonate-rich matrix, BSE image. (**i)** Calcite segregation coexists with phlogopite, Ti-magnetite and perovskite in the matrix, BSE image. Ol = olivine; Phl = phlogopite; Cpx = clinopyroxene; Amp = amphibole; Cr-Spl = Cr-spinel; Prv = perovskite; Ap = apatite; Cal = calcite; Ti-Mag = titanomagnetite; Grt = Ti-rich andradite garnet; Srp = serpentine.

FIGURE 3. BSE (**a**) and QEMSCAN (**b**) images of groundmass minerals in a thin-section from the Wajilitag aillikites. The modal abundance of each mineral phase given in weight percent are converted from volume percent (from the QEMSCAN image) using mineral densities.

FIGURE 4. BSE images and photomicrographs displaying groundmass olivines (**a-c**)

and macrocrysts (**d-f**). (**a-c)** Fine-grained, sub-rounded groundmass olivines with homogeneous compositions distribute in the matrix, BSE image. (**d)** Coarse-grained, anhedral macrocrysts in polygranular dunite nodule, plane-polarized light. (**e)** Areas outlined in **d** display macrocrysts with homogeneous cores and dark Mg-rich rinds with Fo>90, BSE image. (**f)** Monogranular olivine macrocryst distributes in the matrix, BSE image. Ol = olivine, Cpx = clinopyroxene, Ti-Mag = Ti-magnetite.

FIGURE 5. Compositional profiles for representative macrocryst (**a**) and groundmass olivine (**b**). BSE images show orientation and length of EMPA and LA-ICP-MS traverses (red lines). Notice that Fo values of the olivines are measured with EMPA and Ni, Mn, Ca, Ti, Cr and Al concentrations with LA-ICP-MS. Ol = olivine, Cr-Spl = Cr-spinel.

FIGURE 6. Forsterite (Fo) vs. (**a**) Ni, (**b**) Mn, (**c**) Ca, and (**d**) aspect ratio variation for groundmass olivines and macrocrysts from the Wajilitage aillikites. Forsterite contents for the olivines are measured with EMPA and Ni, Mn and Ca with LA-ICP-MS. Note that the Ni, Mn and Ca contents of olivine IIb are from EMPA analyses. The olivine aspect ratios are measured with microscopic analyses. Olivine data from aillikites of the Aillik Bay and Chadobets areas are also included for comparison (Tappe et al. 2006; Veter et al. 2017; Nosova et al. 2018). Kamchatka arc olivine data are from Gavrilenko et al. (2016) and OIB and MORB data from Sobolev et al. (2007).

FIGURE 7. Bivariate plots of LA-ICP-MS for the olivine displaying the compositional differences between groundmass olivines and megacrysts.

FIGURE 8 (**a**) Li vs. Zn, (**b**) Sc vs. Ni, (**c**) Co vs. Ni, and (**d**) Ca vs. Ti (log) for

groundmass olivines and macrocrysts relative to olivine phenocrysts and macrocrysts from aillikites reported by Veter et al. (2017). The fields for 'dry' pyroxenite are from Sobolev et al. (2007) whereas those of phlogopite pyroxenite are based on the chemistry of olivine in lamproites (Ammannati et al. 2016). Fields for olivine chemistry from continental alkaline rocks (basanites, ugandites, melilitites, and kimberlites) and craton peridotite (Sobolev et al. 2007) are also plotted.

FIGURE 9. 100Mn/Fe vs. 100Ni/Mg for the primitive olivine-Ia relative to olivine from aillikites (Veter et al. 2017; Nosova et al. 2018) and orangeites (Howarth 2018). The compositional fields for 'dry' pyroxenite and peridotite are from Sobolev et al. (2007). Geochemical compositions of phlogopite xenocrysts from mantle are after Fritschle et al. (2013).

FIGURE 10 Schematic illustration (not to scale) illustrating the possible evolution of the Wajilitag aillikite magmatic system. See text for detailed descriptions.

Figure 1

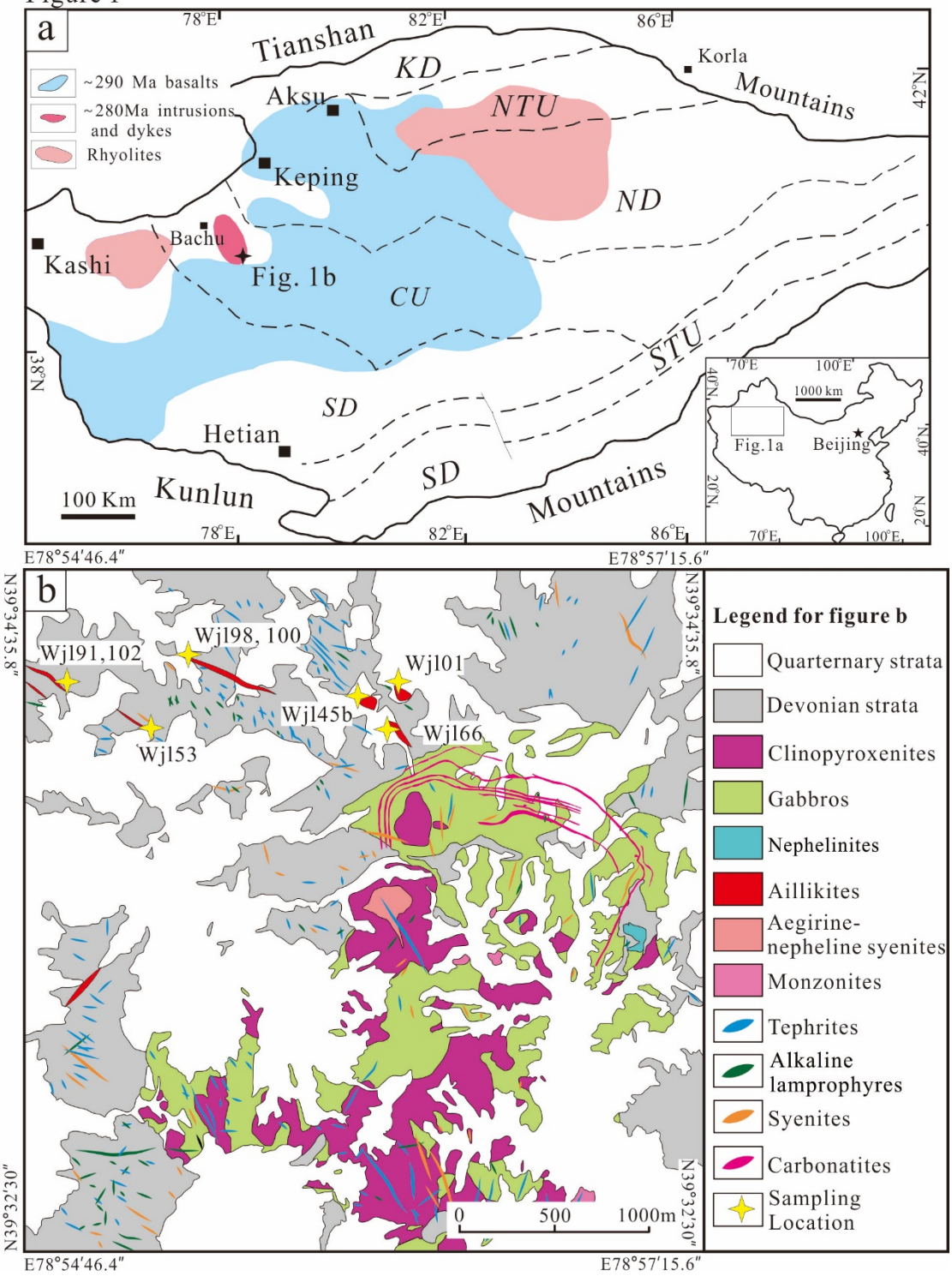

Figure 2

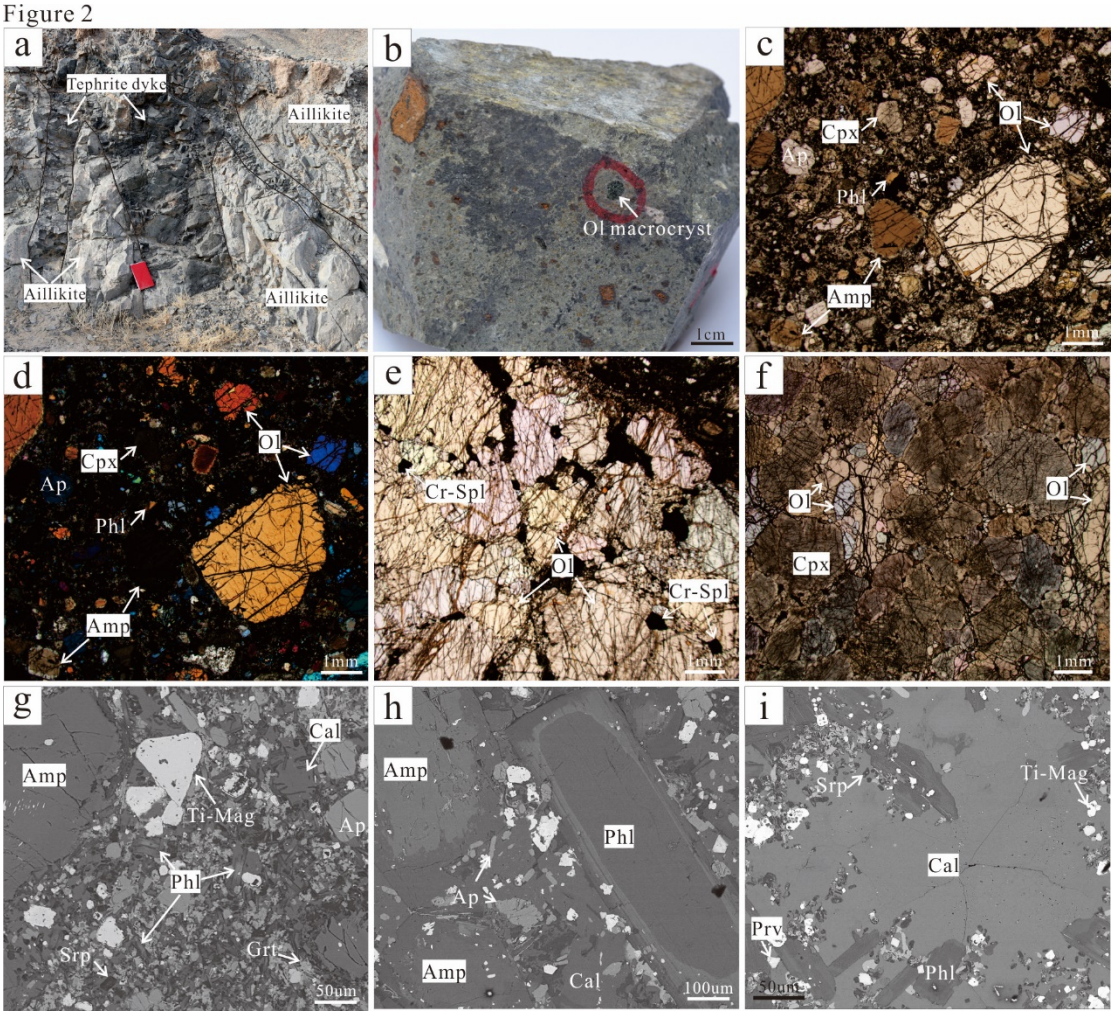

Figure 3

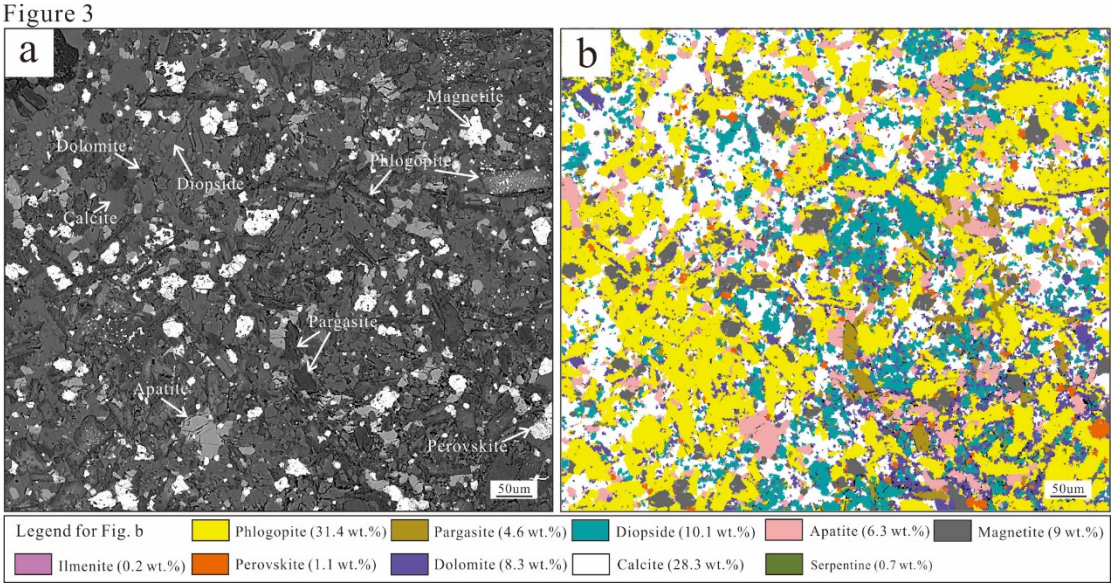

Figure 4

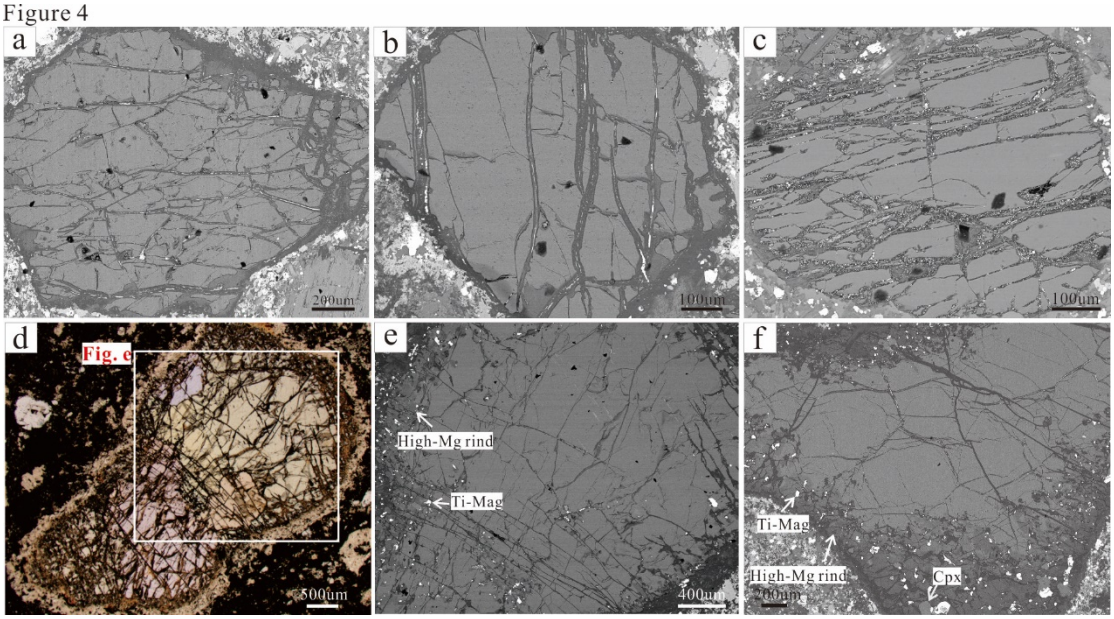

This is the peer-reviewed, final accepted version for American Mineralogist, published by the Mineralogical Society of America.
The published version is subject to change. Cite as Authors (Year) Title. American Mineralogist, in press.
DOI: https://doi.org/10.2138/am-2021-7521. http://www.minsocam.org/

Figure 5

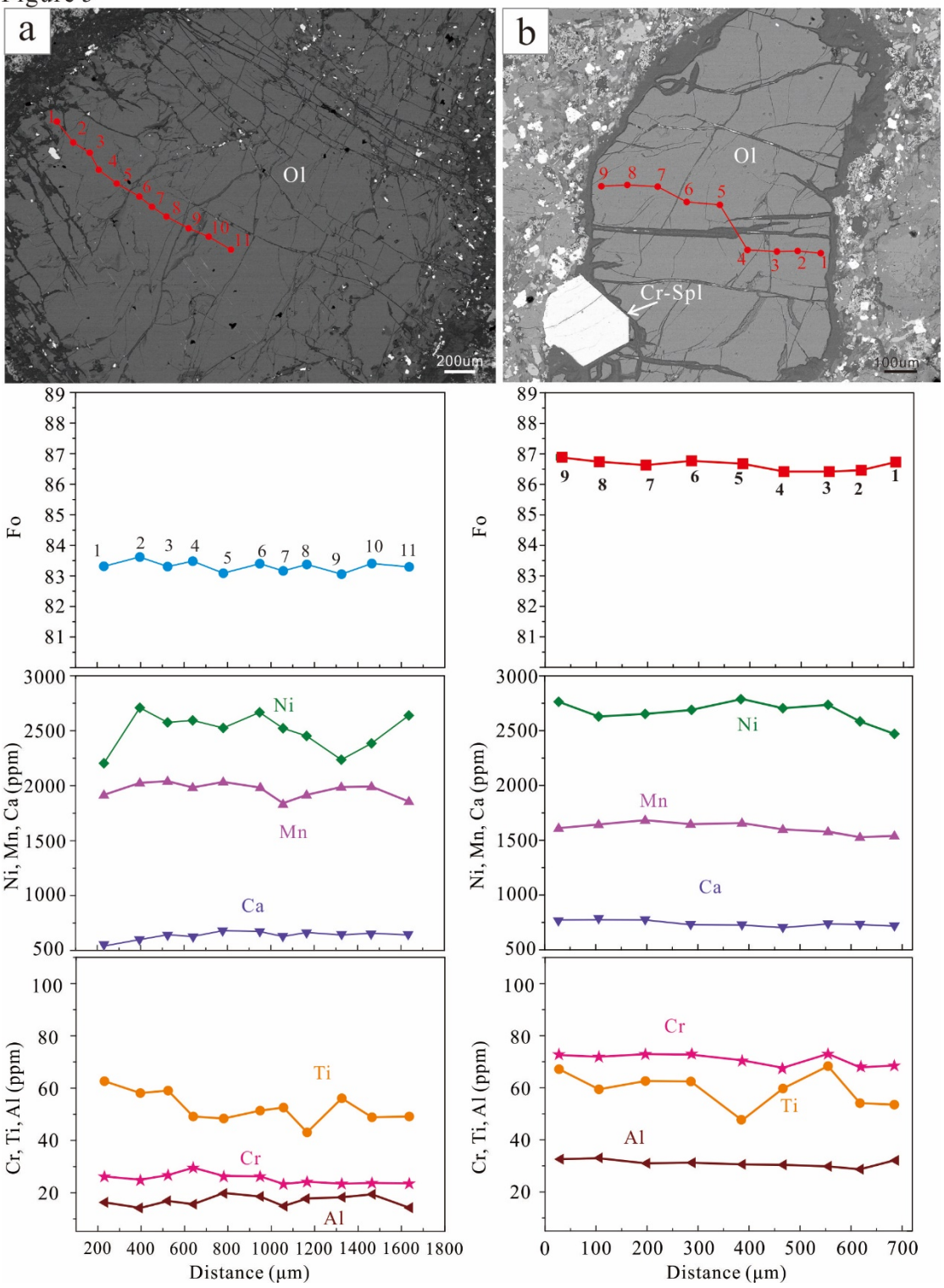

Figure 6

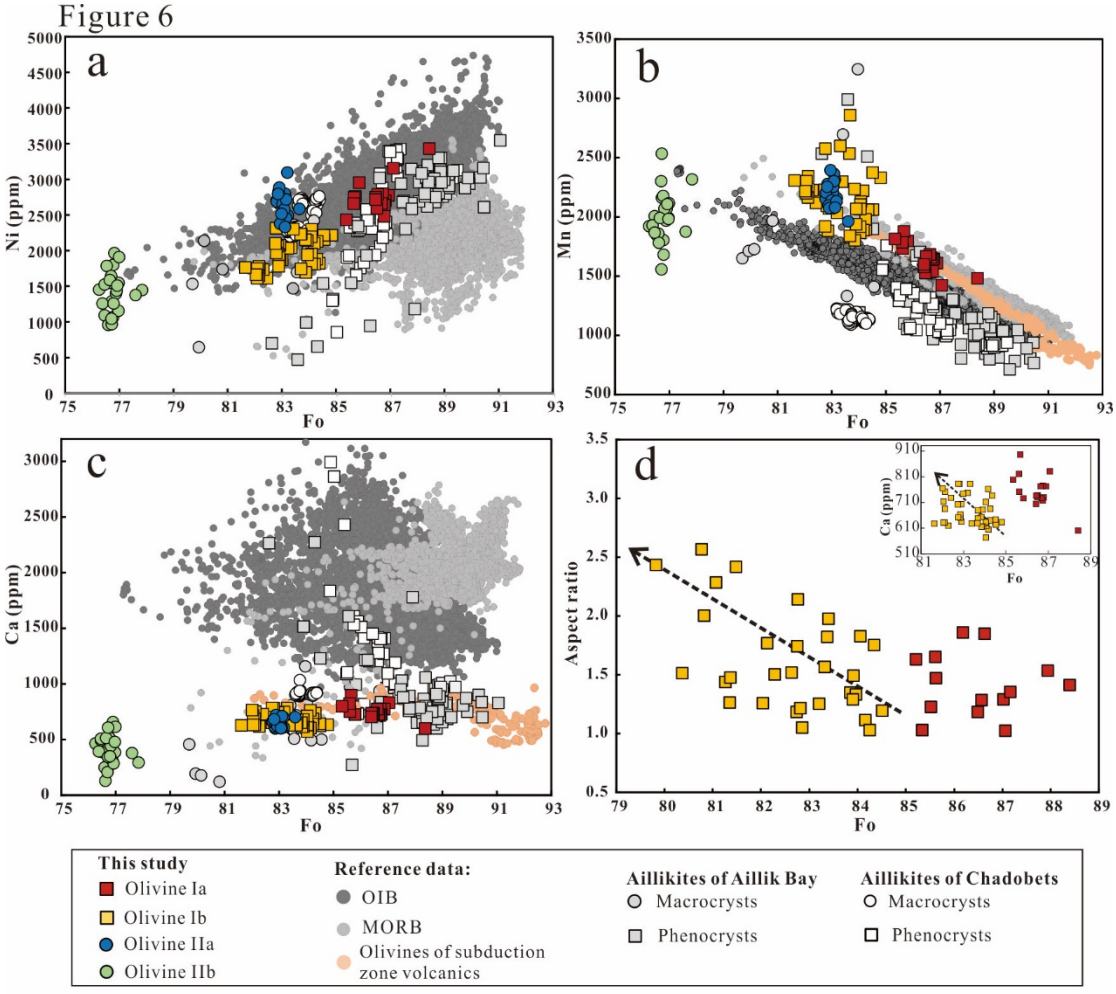

Figure 7

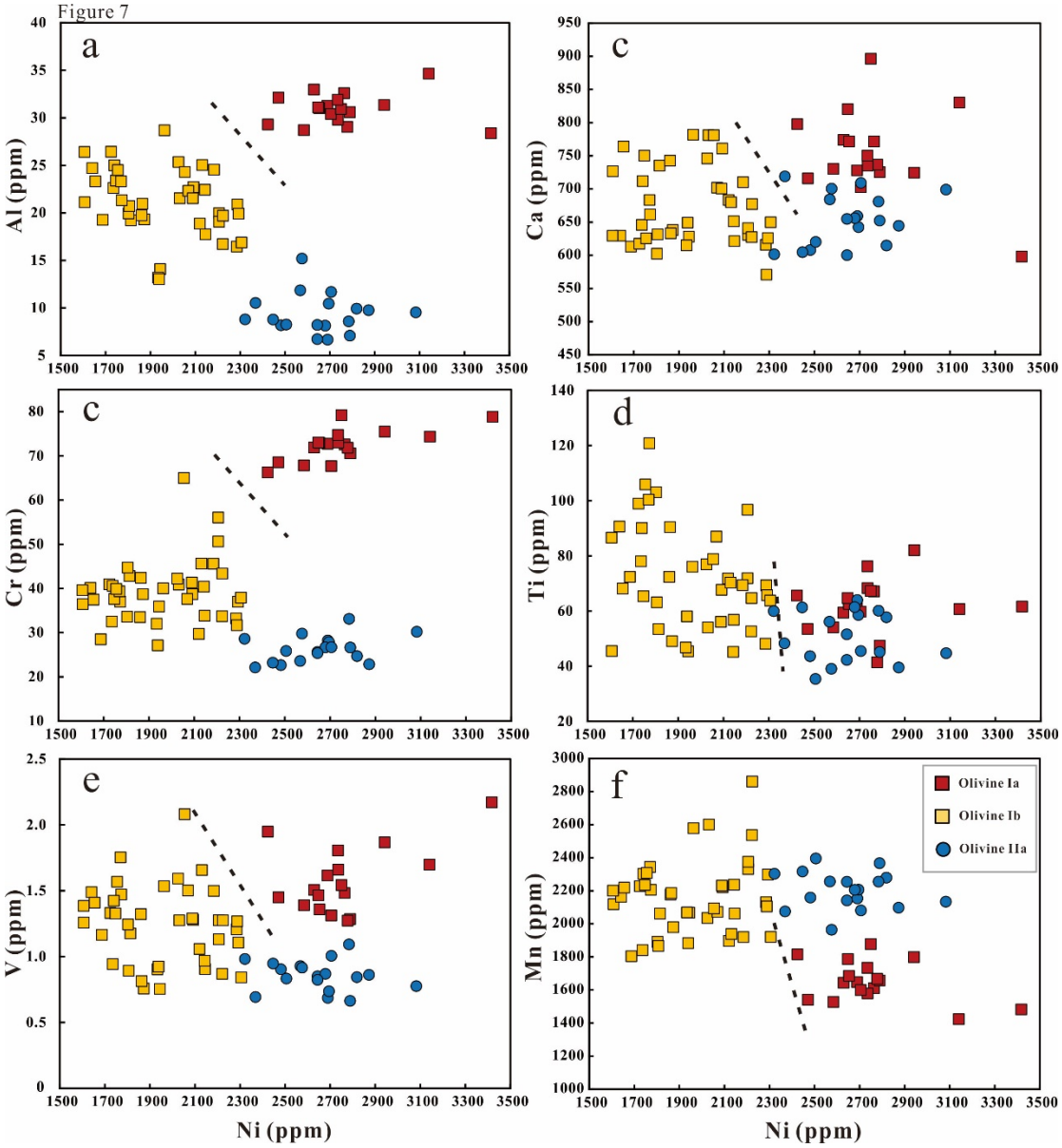

Figure 8

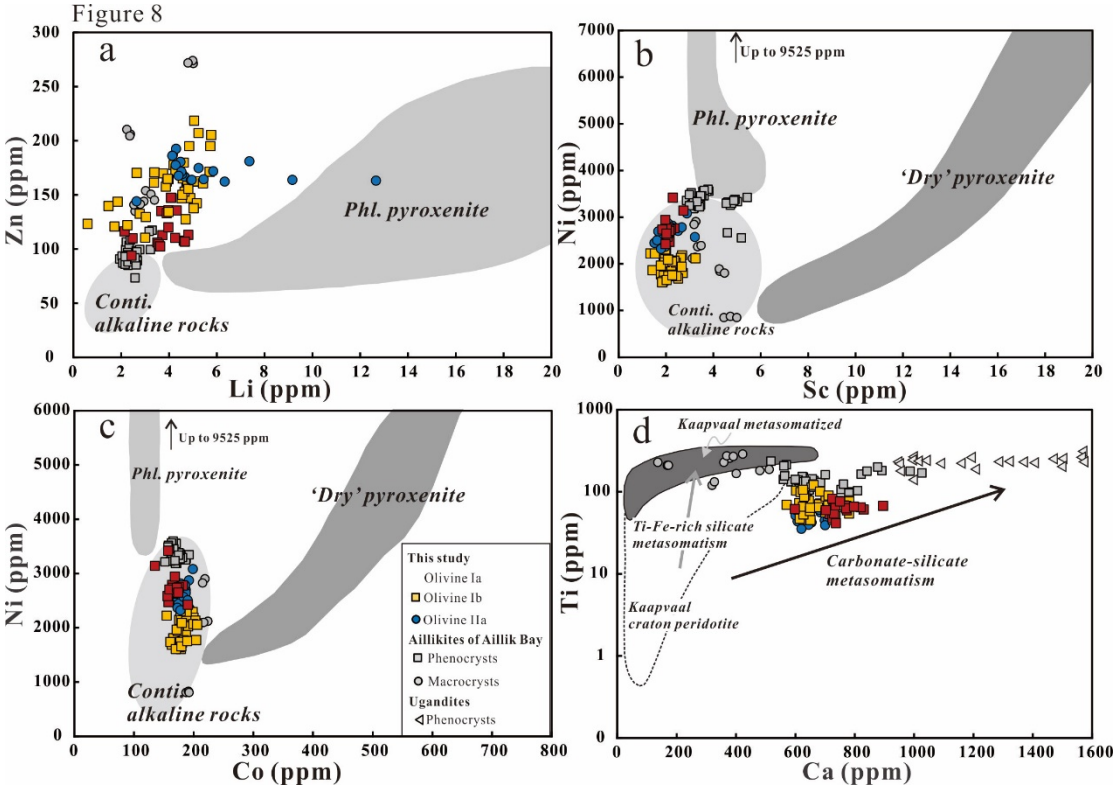

Figure 9

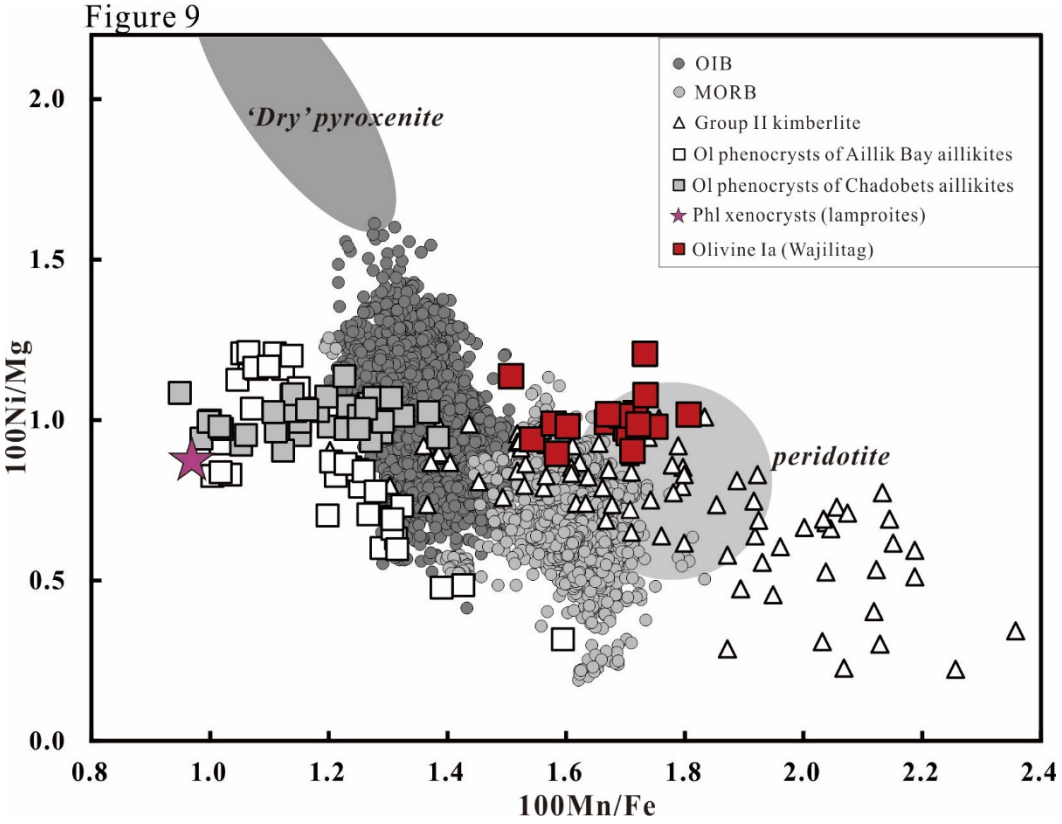

Figure 10